Latin American Journal of Solids and Structures
www.lajss.org

An analytical model of a clamped sandwich beam under low-impulse mass impact

Abstract

An analytical model is developed to examine a low impulsive projectile impact on a fully clamped sandwich beams by considering the coupled responses of the core and the face sheets. Firstly, based on the dynamic properties of foam cores, the sandwich beam is modeled as two rigid perfectly-plastic beams connected by rigid perfectly-plastic springs. Different from the previous sandwich beam model, the transverse compression and bending effects of the foam core are considered in the whole deformation process. Based on this model, different coupling mechanism of sandwich beams are constructed so that an analytical solution considering small deformation is derived. The coupled dynamic responses of sandwich beams with different core strengths are investigated. The results indicate that this model improves the prediction accuracy of the responses of the sandwich beams, and is available for the situation when the sandwich beam undergoes moderate global deformation.

Keywords

sandwich beam, mental foam core, analytical model, low impulse, projectile impact

Wen-zheng Jiang[a]
Ying Liu[a, *]
Yu Gu[a]
G X Lu[b]

[a]Department of Mechanics, School of Civil Engineering, Beijing Jiaotong University, Beijing, 100044
[b]School of Mechanical and Aerospace Engineering, Nanyang Technological University, 50 Nanyang Avenue, Singapore 639798, Singapore

[*]Author e-mail: yliu5@bjtu.edu.cn

1 INTRODUCTION

As one kind of representative structures widely used in the design of commercial and military vehicles, such as aircrafts, spacecrafts, vehicles, ships, and high speed train carriages, responses of sandwich structures subjected to impact at a wide range of velocities have attracted great attention and been extensively studied. How to accurately predict the dynamic behaviors of sandwich structures is of current interest.

For the shock resistance of clamped sandwich beams, Fleck and Deshpande (2004) separate the responses of these beams into three stages, that is, fluid-structure interaction stage; the core compression stage and a combined beam bending and stretching stage. By decoupling these three stages, they develop an analytical model for understanding the blast responses of sandwich beams. In a parallel work, Xue and Hutchinson (2004) compare the blast resistance of clamped sandwich beams to that of monolithic beams of the same mass via three-dimensional finite ele-

ment simulations. Then, some finite element (FE) simulations by Rabczwk *et al.* (2004) and Liang *et al.* (2007) suggest that the model of Fleck and Deshpande may over-estimate or under-estimate the deflection of sandwich beams under blasting loading. This discrepancy indicates that coupling between stages of responses can influence the deflections. Deshpande and Fleck (2005) examine the coupling between the fluid-structure interaction stage I and the core compression stage II. Their results show that the Taylor (1963) analysis based on a free-standing front face-sheet underestimate the transmitted momentum by 20-40% for sandwich beams comprising high strength cores, which explains the discrepancies between the FE simulations of Rabczuk *et al.* (2004) and the analytical predictions of Fleck and Deshpande (2005).

In order to explain the discrepancy between the FE simulation of Liang *et al.* (2007) and the analytical predictions of Fleck and Deshpande (2004), Tilbrook *et al.* (2007) developed an analytical model based on time-scales of core compression and the bending/stretching response of the sandwich beam. In their model, four regimes of behavior, that is, decoupled responses with the sandwich core densification partially or completely, and coupled responses with partial or full core compression, are defined. However, during their formulation, they made one critical assumption, that is, neglecting the shear strength of the core prior to equalization of the velocities of the front and back faces, and the transverse compression strength loads the back and front faces simultaneously. Hence, before the velocity equalization, the sandwich beam is treated approximately as a pressure cavity, which obviously has different deformation mechanism from the structures with foam cores. Following their treatments, some theoretical and experimental works are carried out (Qin, *et al.*, 2009; 2011; Wang, *et al.*, 2011). Although this model to some extend accounts for the coupling between the core compression and the beam bending/stretching phases, their analytical results under-predict the peak back face deflection and over-predict the support reactions, especially for sandwich beams with high strength cores (Tilbrook, *et al.*, 2007).

Structurally, a typical sandwich beam consists of two thin face sheets bonded to a core made from low- density materials. The deformation of the front face under initial dynamic loading, then the core compression and the deflection of the back face, is a series of coupled responding process. The foam core provides not only the transverse pressure, but also the bending/shear strength during the coupled deformation between the core compression and the beam bending/stretching phases. Moreover, researches show that the responses of the foam at the impact or distal ends are different for different impacting conditions (Liu and Zhang, 2009; Liu, *et al.*, 2012), which indicates that the pressures loads on the back and front faces due to the transverse compression of the core may be different, and asynchronous. As a result, how to consider the bending/shear effect of the foam core during the deformation, and describe the transverse pressures on the face sheets caused by the core compression, are the key points in the analytical modeling of sandwich beams, and have not been absolutely solved to per author's knowledge.

Aiming to these problems, an abstracted beam-spring model for the sandwich beam is firstly established by considering the transverse compression and bending effect of the foam core in the whole deformation process. Different from beam-spring system on-rigid foundation (Chen and Yu, 2002; Yu *et al.*, 2002), the coupled motion of the front and back beam is considered. Based on this model, a projectile impact on a fully clamped sandwich beam with a foam core is investigated based on small deflection theory. The coupling deformation mechanism of the beam-spring system

is formulated for sandwich structures with soft or intermediate strength cores. Then the analytical predictions are compared with experimental results and finite element (FE) simulations of the mass impacted sandwich beams to show the availability of this model. At last, the conclusion is given.

2 ANALYTICAL MODEL OF A SANDWICH BEAM UNDER MASS IMPACTING

As shown in Fig. 1a, a fully clamped slender metal foam core sandwich beam impacted by a striker with an initial velocity at the midpoint is considered herein. The mass and the initial velocity of the striker are m_0 and V_0, respectively. The beam length is $2L$. Two face-sheets with thickness h_f and h_b are perfectly bonded to the foam core with the core thickness being C. It is assumed that the face sheet metals obey the rigid-perfectly plastic law with the yield strength is σ_y.

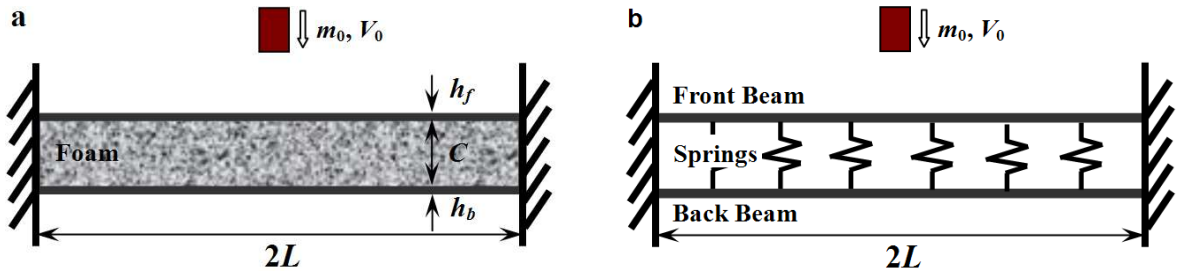

Figure 1 (a) A sandwich beam impacted by a mass; (b) Simplified rigid-perfectly plastic beam-spring model.

In the dynamic analysis we assume that displacements occur only in a direction transverse to the original axis of the beam. Small transverse deflections are considered, such that the deflection w at the mid-span of the beam is assumed to be small compared to the beam length and the rotational inertia is not included into the moment balance equations.

Lopatnikov *et al.* (2007) distinguished the impact/shock loaded cellular solids deformation patterns as two modes, i.e., (a) homogeneous deformation, that is, cellular medium deforms homogeneously over the entire volume of the sample; and (b) progressive collapse, during which the same deformation is reached by complete densification of the portion of the cellular material adjacent to the location where the load applies, while the rest is assumed to be un-deformed. In the present discussion, since small deflection assumption is made and low impulsive loading is considered, homogeneous deformation is assumed which implies the same stress responses at the impact and distal ends of the core. Figure 2 displays a typical stress-strain curve of the cellular material under the dynamic/shock loading, in which σ_0 is the initial force peak, and ε_D and σ_p are densification strain and plateau stress, respectively. Considering that the total outer input energy is greater than the energy absorbed due to the elastic deformation, the rigid perfectly-plastic-locking (RPPL) model is adopted (red line in Fig. 2), and after the densification, the core is treated as rigid.

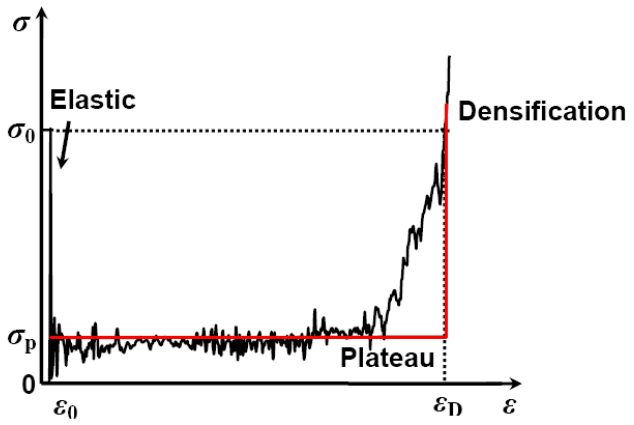

Figure 2 Typical dynamic stress-strain curves for the foam. The red line corresponds to rigid perfectly-plastic-locking (RPPL) model.

Based on this homogeneous deformation assumption of the foam core, rigid-perfectly plastic springs, whose responses obey RPPL model given in Fig. 2, are introduced to establish the relation between the pressures acting on the front and back faces due to the transverse compression of the foam core. Employing the lumped mass approximation, the mass of the core is equally distributed to the front and back beams, that is, the mass per unit length of the front and back faces are (Fleck and Deshpande, 2004)

$$m_f = h_f \rho_f + \rho_c C / 2 \tag{1}$$

and

$$m_b = h_b \rho_b + \rho_c C / 2 \tag{2}$$

where ρ_f, ρ_b, and ρ_c are the densities of the front face, the back face and the foam core, respectively.

In Fig. 3, during the bending of the face sheets, the foam core is also bended. Consequently, except for the transverse pressure, the bending effect of the core should also be considered. Different from Tilbrook *et al.* (2007), in which the shear/bending effect of the core is ignored before the end of the core compression, a simple but critical equivalence is made, that is, the bending moment of the core is divided equally by considering the homogeneous deformation assumption, and added to the corresponding values of the front and back faces to account for the bending effect provided by the foam core. This treatment effectively accounts for the bending effect of the core during the deformation and the validation of this assumption is confirmed via full FE simulation in Section 3. Then we have

$$M_{\mathrm{f}0} = M_{\mathrm{f}} + M_C / 2 = \sigma_y h_f^2 / 4 + M_C / 2 \tag{3}$$

and

$$M_{\mathrm{b0}} = M_{\mathrm{b}} + M_C / 2 = \sigma_y h_b^2 / 4 + M_C / 2 \tag{4}$$

where M_{f}, M_{b}, and M_C are the sectional limit bending moments of the front face, the back face and the foam core, respectively, in which

$$M_{\mathrm{C}} = \sigma_{yC} C^2 \left(1 - \varepsilon_m\right)^2 / 4 \tag{5}$$

where σ_{yC} is the yield strength of the foam core, ε_m is the middle point compression strain which is defined as $\varepsilon_m = |W_f - W_b| / C$ with W_f and W_b the mid-span deflections of the front and back beams, respectively.



Figure 3 Experimental results of impact failure modes with respect to load intensity (Wang, *et al.*, 2011).

By now, the sandwich beam is modeled as two beams with larger mass and bending moments (compared to the face sheets) connected by rigid-perfectly plastic springs, which is shown in Fig. 1b. After the deformation of the front beam, the forces due to the compression of the foam core will act on the back beam. If the core is sufficiently strong, it will decelerate the front beam and simultaneously accelerate the back beam; otherwise, the back beam will keep un-deformed at the plateau stage of the core compression. The response of the clamped beam depends on the transverse pressure s_{p} acting from the core onto the back face. Following Jones (1989), by taking $\gamma = \sigma_p / \sigma_{bs}$ with $\sigma_{bs} = 4M_{\mathrm{b0}} / L^2$ the static extreme pressure of the back beam with $\varepsilon_m = 0$, the sandwich beam with intermediate or low strength cores are considered in the following section.

2.1 Intermediate strength foam core ($1 \le \gamma \le 3$)

When the front beam is impacted, the midpoint of the beam moves with the velocity V_0 at the instantaneous impact, whilst the left part keeps stationary. In order to keep balance, a disturbance is propagated along the beam from the midpoint to the fixed ends and the core is gradually compressed. This includes two different kinematical phases: a transient phase ($0 \le t \le t_{\mathrm{I}}$, phase I, Fig. 4a), and a modal phase ($t_{\mathrm{I}} < t \le t_{\mathrm{II}}$, phase II, Fig. 4b). At the same time, the back beam will also deform since the plateau stress of the core is assumed to be greater than its yield stress (γ>1). Corresponding to the kinematical phases of the front beam, the deformation of the back beam includes the deflection under a moving and then a uniform loading (Figs. 5a and 5b), respectively. When the velocities of the front and back beams become the same (t=t_{eq}), the beams deform as a system, as shown in Fig. 6 ($t \ge t_{\mathrm{eq}}$, phase III). Moreover, if the densification (t=t_{D}) is reached before the equivalent velocity is obtained ($t_{\mathrm{D}} \le t \le t_{\mathrm{eq}}$), the front and back beams also begin to deform as a system (phase III).

2.1.1 Coupled deformation in the first phase, $0 \le t \le t_{\mathrm{I}}$

2.1.1.1 Front beam

In the first phase, a disturbance propagates from the central point to the fixed ends. Because of symmetry, the right half beam $0 \le x \le L$ is considered. Its transverse velocity field is assumed to be (Figs. 4a and 4b)

$$\begin{aligned} \dot{w}_{f1} &= \dot{W}_{f1}(1 - x/\xi) \qquad 0 \le x \le \xi, \\ \dot{w}_{f1} &= 0 \qquad\qquad\qquad\quad \xi \le x \le L, \end{aligned} \tag{6}$$

where w is the transverse displacement, ξ is the position of the plastic hinge which dependents on the time t. The upper dot means the differentiating with respect to the time t, and the suffix f represents the front beam and the number 1 the first phase. At the moving plastic hinges (x=$\pm\xi$), the bending moment M_{f1} is maximum and the transverse force Q=0. The force balance between the two moving plastic hinges along the transverse direction yields

$$m_0 \ddot{W}_{f1} + 2\int_0^{\xi} m_f \ddot{w}_{f1} dx + 2\int_0^{\xi} q(x)\, dx = 0 \tag{7}$$

where $q(x)$ is the dynamic pressure caused by the compression of the foam core, which keeps constant before densification as shown in Fig.2 (red line).

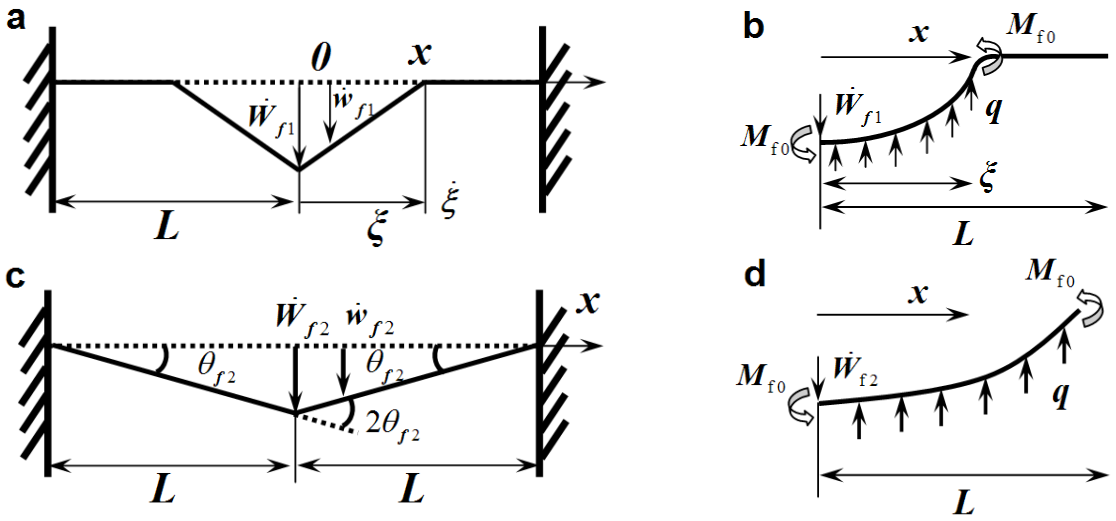

Figure 4 (a) Velocity profile of the front beam in phase I; (b) a free body diagram of the left half front beam in phase I; (c) velocity profile of the front beam in phase II; (d) a free body diagram of the left half front beam in phase II.

Substitution Eq. (6) into Eq. (7) leads to

$$m_0\ddot{W}_{f1}+2m_f\int_0^{\xi}\ddot{W}_{f1}(1-x/\xi)dx+2\int_0^{\xi}q(x)dx=0 \tag{8}$$

that is,

$$m_0\ddot{W}_{f1}+m_f\left(\ddot{W}_{f1}\xi+\dot{W}_{f1}\dot{\xi}\right)=-2\int_0^{\xi}q(x)dx \tag{9}$$

Considering the moment balance between x=0 and x=ξ to the beam midpoint, and the boundary conditions: M_{f1}=M_{f0} at x=0; M_{f1}= -M_{f0} and Q=0 at x=L, we have

$$2M_{f0}-\int_0^{\xi}m_f\ddot{w}_{f1}xdx-\int_0^{\xi}q(x)x\,dx=0 \tag{10}$$

Substitution Eqs. (6) into Eq. (10) and considering $q(x)$=σ_p yields

$$2M_{f0}-m_f\left(\ddot{W}_{f1}\xi^2/6+\dot{W}_{f1}\dot{\xi}\xi/3\right)-\sigma_p\xi^2/2=0 \tag{11}$$

Then we have

$$\frac{d\left(\dot{W}_{f1}\xi^2\right)}{dt}=(12M_{f0}-3\sigma_p\xi^2)/m_f \tag{12}$$

Integrating Eq. (12) and considering when t=0, ξ=0, we have

$$t = \frac{m_f \dot{W}_{f1} \xi^2 + 3\sigma_p \int_0^t \xi^2 \, dt}{12 M_{f0}} \tag{13}$$

Integrating Eq. (9) and considering when t=0, ξ=0, and $\dot{W}_{f1} = V_0$, we have

$$\dot{W}_{f1} = \frac{m_0 V_0 - 2\int_0^t \sigma_p \xi \, dt}{m_0 + m_f \xi} \tag{14}$$

Combination Eqs. (13) and (14) we have the time-position relation of the dynamic plastic hinge, that is

$$t = \frac{m_f \xi^2 \left(m_0 V_0 - 2\sigma_p \int_0^t \xi \, dt \right)}{12 M_{f0} \left(m_0 + m_f \xi \right)} + \frac{\sigma_p \int_0^t \xi^2 \, dt}{4 M_{f0}} \tag{15}$$

Differentiating Eq. (15) with respect to the time t, we obtain the travelling velocity of the plastic hinge, that is,

$$\dot{\xi} = \frac{2 m_f \sigma_p \xi^3 \left(m_0 + m_f \xi \right) + \left(12 M_{f0} - 3\sigma_p \xi^2 \right) \left(m_0 + m_f \xi \right)^2}{m_f \xi \left(2 m_0 + m_f \xi \right) \left(m_0 V_0 - 2\sigma_p \int_0^t \xi \, dt \right)} \tag{16}$$

When the plastic hinge arrives at the fixed end, we have ξ=L, that is, t=t_I, the first phase ends. According to Eqs. (14) to (16), we can obtain the related deformation parameters of the front beam in the first phase. It is seen that x is time and position dependent. The direct integrals of Eqs. (14) to (16) are impossible. Numerical integration using MatLab is performed. Moreover, as expected when σ_p=0, Eqs. (14) to (16) degenerate to the equations for monoclinic beams given in Appendix A. Comparison between Eq. (14) and Eq. (A6) indicates that the velocity of the mid-span point of the front beam is smaller than that of the monolithic beam due to the existence of the foam core.
In the first phase, the kinetic energy of the mass and the front beam is

$$E_{fI} = E_{mass} + E_{front} = \frac{m_0 \dot{W}_{f1}^2}{2} + \frac{m_f \dot{W}_{f1}^2 \xi}{3} \tag{17}$$

When the moving plastic hinge length is ξ, the dissipated plastic bending energy is

$$U_{\text{Bending-FI}} = \frac{4M_{\text{f0}}W_{f1}}{\xi} \tag{18}$$

and the dissipated spring potential energy is

$$U_{\text{Spring-FI}} = 2\int_0^{\xi} \sigma_{\text{p}} \Delta w_{f1}\, dx \tag{19}$$

where Δw_{f1} is the relative deflection of the front beam at point x.

2.1.1.2 Back beam

Because $\gamma>1$, during the deformation of the front beam, the back beam also deforms. According to experimental and numerical examination, the transverse velocity field of the back beam in the first phase is assumed as (Figs. 5a and 5b)

$$\begin{aligned} \dot{w}_{b1} &= \dot{W}_{b1}(1-x/\xi) \qquad 0 \le x \le \xi, \\ \dot{w}_{b1} &= 0 \qquad\qquad\qquad\quad \xi \le x \le L, \end{aligned} \tag{20}$$

and the governing equations of the beam are

$$\frac{\partial^2 M_{b1}}{\partial^2 x} = -\sigma_{\text{p}} + m_b \frac{\partial^2 w_{b1}}{\partial^2 t} \qquad 0 \le x \le \xi \tag{21a}$$

$$\frac{\partial^2 M_{b1}}{\partial^2 x} = 0 \qquad \xi < x \le L \tag{21b}$$

where M_{b1} is the bending moment of the back beam at the first stage.

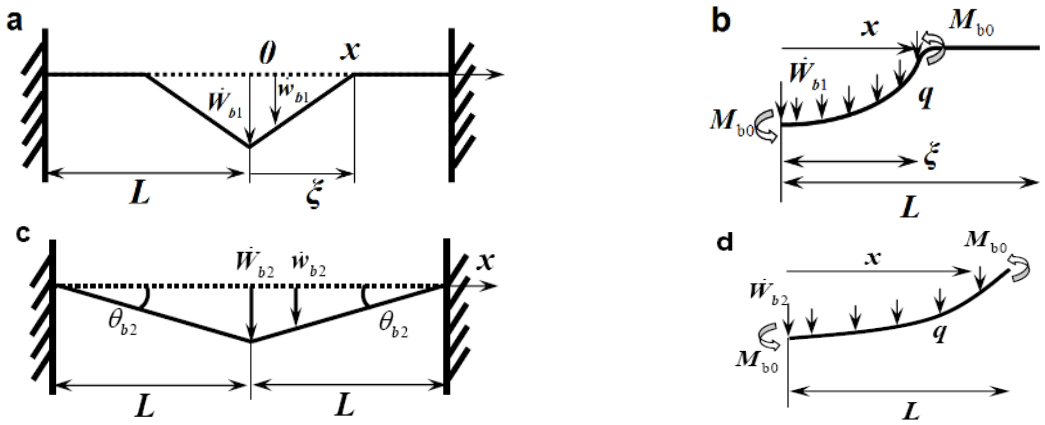

Figure 5 (a) Velocity profile of the back beam in phase I; (b) a free body diagram of the left half back beam in phase I; (c) velocity profile of the back beam in phase II; (d) a free body diagram of the left half back beam in phase II.

Substitution Eq. (20) into Eq. (21a) leads to

$$\frac{\partial^2 M_{b1}}{\partial^2 x} = -\sigma_{\mathrm{p}} + m_b(1 - x/\xi)\frac{d^2 W_{b1}}{d^2 t} \qquad 0 \le x \le \xi \tag{22}$$

Integrating Eq. (22) and considering $M_{b1} = M_{\mathrm{b0}}$, $Q = \partial M_{b1}/\partial x = 0$ at x=0, we have

$$M_{b1} = -\sigma_{\mathrm{p}} x^2/2 + m_b(x^2/2 - x^3/6\xi)\frac{d^2 W_{b1}}{d^2 t} + M_{\mathrm{b0}} \quad 0 \le x \le \xi \tag{23}$$

Since at x=ξ, M_{b1}=-M_{b0}, according to Eq. (23), we have

$$\frac{d^2 W_{b1}}{d^2 t} = (3\sigma_{\mathrm{p}}\xi^2/2 - 6M_{\mathrm{b0}})/m_b\xi^2 \tag{24}$$

It should be pointed out that for beams under the moving loading, the assumed velocity field is only valid for

$$\sigma_{\mathrm{p}} \ge \frac{4M_{\mathrm{b0}}}{L\xi} \tag{25}$$

which leads to

$$\xi \ge \frac{4M_{b0}}{L\sigma_{\mathrm{p}}} \tag{26}$$

As a result, the back beam does not deform simultaneously with the front beam. Only after Eq. (26) is satisfied does the back beam begins to deform.
Integration Eq. (24) leads to

$$\dot{W}_{b1} = \left(3\sigma_{\mathrm{p}}\xi^2/2 - 6M_{\mathrm{b0}}\right)t/m_b\xi^2 \tag{27}$$

In Fig. 5a, when the moving hinges arrive at the fixed ends, that is, $\xi = L$, the moving forces arrive at the fixed ends and the first stage ends. The kinetic energy of the back beam in the first phase is

$$E_{\mathrm{BI}} = \frac{m_b \dot{W}_{b1}^2 \xi}{3} \tag{28}$$

When the length of the moving pressure $x=x$, the dissipated plastic bending energy is

$$U_{\text{Bending-BI}} = \frac{4M_{\text{b0}}W_{b1}}{\xi} \tag{29}$$

and the dissipated spring potential energy is

$$U_{\text{BSpringI}} = 2\int_0^{\xi} \sigma_{\text{p}} \Delta w_{b1} dx \tag{30}$$

where Δw_{b1} is the relative deflection of the back beam at point x.

2.1.2 Coupled deformation in the second phase, $t_{\text{I}} < t \leq t_{\text{II}}$

In the second phase, the plastic hinges are fixed during which the remaining energy is dissipated by the plastic deformation of the plastic hinges (Fig. 4c), the foam core and the deformation of the back beam (Fig. 5c).

2.1.2.1 Front beam

Seen as Fig. 4c, we assume the transverse velocity field of the front beam in the second phase is

$$\dot{w}_{f2} = \dot{W}_{f2}(1 - x/L) \qquad 0 \leq x \leq L \tag{31}$$

The governing equation of the beam is

$$\frac{\partial^2 M_{f2}}{\partial^2 x} = \sigma_{\text{p}} + m_f \left(1 - x/L\right) \frac{d^2 W_{f2}}{d^2 t} \qquad 0 \leq x \leq L \tag{32}$$

Integrating Eq. (32) and considering $M_{f2} = M_{\text{f0}}$, $Q = m_0 \ddot{W}_{f2}/2$ at $x=0$, we have

$$\frac{\partial M_{f2}}{\partial x} = \sigma_{\text{p}} x + m_f \left(x - \frac{x^2}{2L}\right) \frac{d^2 W_{f2}}{d^2 t} + \frac{m_0}{2} \frac{d^2 W_{f2}}{d^2 t} \qquad 0 \leq x \leq L \tag{33}$$

and

$$M_{f2} = \sigma_{\text{p}} x^2/2 + m_f \left(\frac{x^2}{2} - \frac{x^3}{6L}\right) \frac{d^2 W_{f2}}{d^2 t} + \frac{m_0}{2} \frac{d^2 W_{f2}}{d^2 t} x + M_{\text{f0}} \qquad 0 \leq x \leq L \tag{34}$$

Considering $M_{f2} = -M_{\text{f0}}$ at $x=L$, we have

$$\ddot{W}_{f2} = -\frac{12M_{f0} + 3\sigma_p L^2}{2m_f L^2 + 3m_0 L} \tag{35}$$

Integrating Eq. (35) leads to

$$\dot{W}_{f2} = -\frac{12M_{f0} + 3\sigma_p L^2}{2m_f L^2 + 3m_0 L} t + \dot{W}_{f1} \tag{36}$$

where $\dot{W}_{f1}$ is the mid-span velocity of the front beam at the end of the first phase.

In the second phase, the kinetic energy of the front beam and the mass is

$$E_{FII} = E_{mass} + E_{front} = \frac{m_0 \dot{W}_{f2}^2}{2} + \frac{m_f \dot{W}_{f2}^2 L}{3} \tag{37}$$

For the front beam, the dissipated plastic bending energy is

$$U_{\text{Bending-FII}} = \frac{4M_{f0} W_{f2}}{L} \tag{38}$$

and the dissipated spring potential energy is

$$U_{\text{FSpringII}} = 2\int_0^L \sigma_p \Delta w_{f2} \, dx \tag{39}$$

where Δw_{f2} is the relative deflection of the front beam at point x.

2.1.2.2 Back beam

As shown in Fig. 5c, we assume the transverse velocity field of the back beam in the second phase is

$$\dot{w}_{b2} = \dot{W}_{b2}(1 - x/L) \tag{40}$$

and the governing equation of the beam is

$$\frac{\partial^2 M_{b2}}{\partial^2 x} = -\sigma_p + m_b\left(1 - x/L\right)\frac{d^2 W_{b2}}{d^2 t} \qquad 0 \le x \le L \tag{41}$$

Integrating Eq. (41) and considering $M_{b2} = M_{b0}$, $Q = \partial M_{b2}/\partial x = 0$ at x=0, we have

$$\frac{\partial M_{b2}}{\partial x} = -\sigma_{\mathrm{p}} x + m_b \left(x - \frac{x^2}{2L} \right) \frac{d^2 W_{b2}}{d^2 t} \qquad 0 \le x \le L \tag{42}$$

and

$$M_{b2} = -\sigma_{\mathrm{p}} x^2 / 2 + m_b \left(\frac{x^2}{2} - \frac{x^3}{6L} \right) \frac{d^2 W_{b2}}{d^2 t} + M_{\mathrm{b0}} \qquad 0 \le x \le L \tag{43}$$

Considering $M_{b2} = -M_{\mathrm{b0}}$ at $x=L$, we have

$$\ddot{W}_{\mathrm{b2}} = \left(3\sigma_{\mathrm{p}} L^2 - 12 M_{\mathrm{b0}} \right) \Big/ \left(2 m_b L^2 \right) \tag{44}$$

Integrating Eq. (44) leads to

$$\dot{W}_{\mathrm{b2}} = \left(3\sigma_{\mathrm{p}} L^2 - 12 M_{\mathrm{b0}} \right) t \Big/ \left(2 m_b L^2 \right) + \dot{W}_{b\mathrm{I}} \tag{45}$$

where $\dot{W}_{b\mathrm{I}}$ is the velocity of the middle point of the back beam at the end of the first phase.

Then the kinetic energy of the back beam in the second phase is

$$E_{\mathrm{BII}} = \frac{m_{\mathrm{b}} L \dot{W}_{b2}^2}{3} \tag{46}$$

The dissipated plastic bending energy is

$$U_{\text{Bending-BII}} = \frac{4 M_{\mathrm{b0}} W_{b2}}{L} \tag{47}$$

The dissipated spring potential energy is

$$U_{\mathrm{BSpringII}} = 2 \int_0^L \sigma_{\mathrm{p}} \Delta w_{b2} \, d x \tag{48}$$

where Δw_{b2} is the relative deflection of the back beam at point x in the phase II.

2.1.3 Coupled deformation in the third phase, ($t \ge t_{\mathrm{eq}}$, or $t_{\mathrm{D}} \le t \le t_{\mathrm{eq}}$)

In the first and second phases, the front beam makes decelerated motion, while the back beam has accelerated motion. If core densification is not reached, the front and back beams will arrive at the same velocity at time $t=t_{\mathrm{eq}}$, after which the sandwich beam deforms as one single beam as shown in Fig. 6, which is referred as phase III.

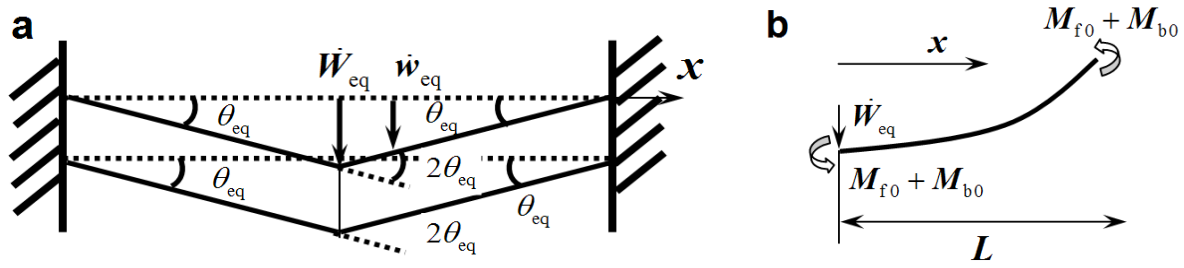

Figure 6 (a) Velocity profile of the beams in phase III- system deformation; (b) a free body diagram of the left half beams in phase III- system deformation.

At that time, we assume the velocity field of the sandwich beam with the form

$$\dot{w}_{III} = \dot{W}_{III}(1 - x/L) \qquad 0 \le x \le L \tag{49}$$

and the governing equation

$$\frac{\partial^2 M_{III}}{\partial^2 x} = \left(m_f + m_b\right)(1 - x/L)\frac{d^2 W_{III}}{d^2 t} + m_0 \frac{d^2 W_{III}}{d^2 t} \qquad 0 \le x \le L \tag{50}$$

Integrating Eq. (50) and considering $M_{eq} = M_{f0} + M_{b0}$, $Q = \partial M_{III}/\partial x = 0$ at x=0, we have

$$M_{III} = \left(m_f + m_b\right)(x^2 - x^3/6L)\frac{d^2 W_{eq}}{d^2 t} + \frac{m_0 x^2}{2}\frac{d^2 W_{eq}}{d^2 t} + M_{eq} \qquad 0 \le x \le L \tag{51}$$

Considering M_{III}= -M_{eq} at x=L, we have

$$\ddot{W}_{eq} = -\frac{12 M_{eq}}{2\left(m_f + m_b\right)L^2 + 3m_0 L^2} \tag{52}$$

Integration Eq. (52) yields

$$\dot{W}_{III} = \dot{W}_{eq} - \frac{12 M_{eq}}{2\left(m_f + m_b\right)L^2 + 3m_0 L^2} t \tag{53}$$

If the densification occurs at t=t_D before the common velocity of the faces is reached, the sandwich beam directly deforms as in phase III, which is governed by Eqs. (52) and (53). At that time, $\dot{W}_{eq}$ is determined by the momentum balance. If the densification occurs in the first phase of the front and back beams, we have

$$m_0\dot{W}_f + \int_0^{\xi} 2m_f\,\dot{w}_f\Big|_{t=t_D} dx + \int_0^{\xi} 2m_b\,\dot{w}_b\Big|_{t=t_D} dx = m_0\dot{W}_{\text{eq}} + \int_0^{\xi} 2\left(m_f + m_b\right)\dot{w}_{\text{eq}} dx \tag{54a}$$

and in the second phase, we have

$$m_0\dot{W}_f + \int_0^{L} 2m_f\,\dot{w}_f\Big|_{t=t_D} dx + \int_0^{L} 2m_b\,\dot{w}_b\Big|_{t=t_D} dx = m_0\dot{W}_{\text{eq}} + \int_0^{L} 2\left(m_f + m_b\right)\dot{w}_{\text{eq}} dx \tag{54b}$$

The kinetic energy of system in the phase III is

$$E_{\text{III}} = E_{mass} + E_{front} + E_{back} = \frac{m_0\dot{W}_{\text{eq}}^2}{2} + \frac{\left(m_f + m_b\right)L\dot{W}_{\text{eq}}^2}{3} \tag{55}$$

The dissipated plastic bending energy is

$$U_{\text{Bending-III}} = \frac{4\left(M_{\text{f0}} + M_{\text{b0}}\right)W_{\text{eq}}}{L} \tag{56}$$

Since the core is not compressed in the Phase III, the energy dissipated by springs is zero.

2.2 Low strength core ($\gamma < 1$)

In this case, if all of the energy is dissipated before the core densification is reached, the back beam will not deform and the final deflection of the upper beam could be obtained according to the equations given in section 2.1.1.1 and 2.1.2.1 for the front beam. If the densification is reached, the deformation of the beams will follow Eqs. (52), (53), and (54).

2.3 Non-dimensional groups

Following Tilbrook *et al.* (2007), we use the same independent and dependent non-dimensional groups.

The non-dimensional geometric variables of the sandwich beam are

$$\bar{C} = \frac{C}{L},\ \bar{h} = \frac{h_f + h_b}{2C},\ \tilde{h} = \frac{h_b}{h_f} \tag{57}$$

and the non-dimensional core properties are ε_D,

$$\bar{\rho} = \frac{\rho_c}{\rho_f},\ \bar{\sigma}_{yC} = \frac{\sigma_{yC}}{\bar{\rho}\sigma_y} \tag{58}$$

For the impulse, it is defined as

$$\bar{I} = I \Big/ L\sqrt{\rho_f \sigma_y} \tag{59}$$

In addition, the dependent non-dimensional groups are

$$\bar{t} = \frac{t}{\tau},\ \bar{w}_f(\bar{t}) = \frac{w_f}{L},\ \bar{w}_b(\bar{t}) = \frac{w_b}{L},\ \bar{W}_f = \frac{W_f}{L},\ \bar{W}_b = \frac{W_b}{L},\ \bar{v}_f(\bar{t}) = \frac{v_f \rho_f h_f}{I},\ \text{and}$$
$$\bar{v}_b(\bar{t}) = \frac{v_b \rho_f h_f}{I} \tag{60}$$

where $\tau = L \Big/ \sqrt{\sigma_y / \rho_f}$ is the response time of a plastic string of length $2L$ made from a material with yield strength σ_y and density ρ_f.

3 DYNAMIC RESPONSE IN TERMS OF DEFLECTION

For the sandwich beams under blasting loading, Liang *et al.* (2007) divides their behaviors into three regimes by comparing various time-scales in the responses, which is given in Fig. 7. In the figures, t_{bd} is the time at which the back face begins to decelerate, and t_{eq} is the time that the mid-span velocities of the front and back faces are equal. Following their definition, explicit finite element analysis is performed and the results are compared with the analytical study. In the FE model, the face sheets and the core are assumed perfectly bonded together. Element type Solid164, an 8-node solid structural element provided by the code (LS-DYNA, 2007) is used to discretize the face sheets and the foam core. There are 4050 and 10125 elements for the face sheets and the foam core of the beam, respectively. The vertical, horizontal and rotational displacements of nodes at the ends of the beam are zero. Appropriate mesh refinements near the impact point and the end support are included. Mesh sensitivity is checked before calculations. The automatic time step calculation option from the code is chosen. The contact between the beam and the roller is modeled by using a contact pair surface algorithm with a frictionless contact option (LS-DYNA, 2007).

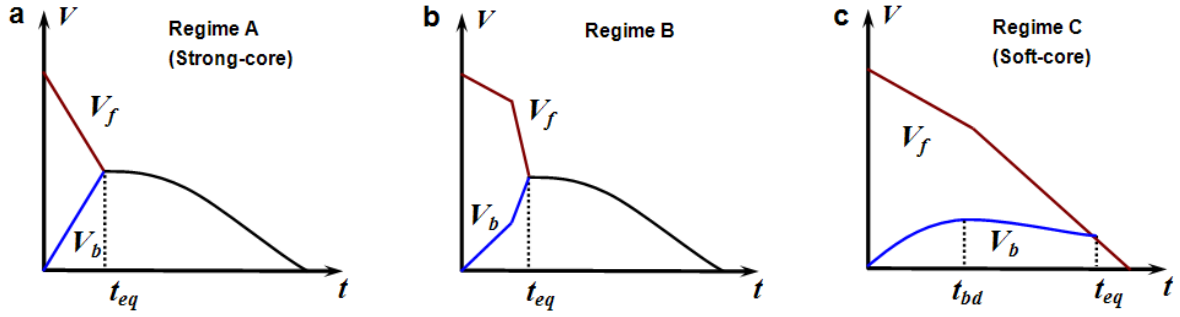

Figure 7 Velocity versus time histories of the mid-span of the front and back faces in three regimes: regime A- strong core; regime B- densification reaches before the velocities equalization; regime C- soft core [4].

Firstly the analytical prediction and experimental results are compared. Following Wang *et al.* (2011), the material and geometrical parameters of sandwich beams are listed in Table 1. The striker mass is equal to the mass of the foam projectile used in experiments. Fig. 8 shows the experimental results and our analytical prediction for the normalized maximum middle point deflection of the back face. It is seen that when the core makes the large global deformation, our prediction agrees well with the experimental ones. But when the core shear or fractures was present in the experiments of the sandwich structures, which is not considered in the analytical modeling, the deviation of our predictions from the experimental results increases. Nevertheless, during the global deformation stage, our model could well predict the experimental results.

Table 1 Material parameters of sandwich beams

	Symbol	Value
Beam length	$2L$	250 mm
Mass of projectile	m_0	0.0125 kg
Face-sheet thickness	h_f and h_b	0.5 mm
Thickness of metal foam core/ aluminum honeycomb core	C	10 mm/12.5 mm
Tensile strength of face sheets	σ_y	75.8 MPa
Density of face sheets	ρ_f and ρ_b	2700 kg/m^3
Density of metal foam core/ aluminum honeycomb core	ρ_c	270 kg/m^3/86.4 kg/m^3
Compressive strength of metal foam core/ aluminum honeycomb core	σ_{yC}	2.0 MPa/1.0 MPa
Densification strain of metal foam core/ aluminum honeycomb core	ε_D	0.7/0.8

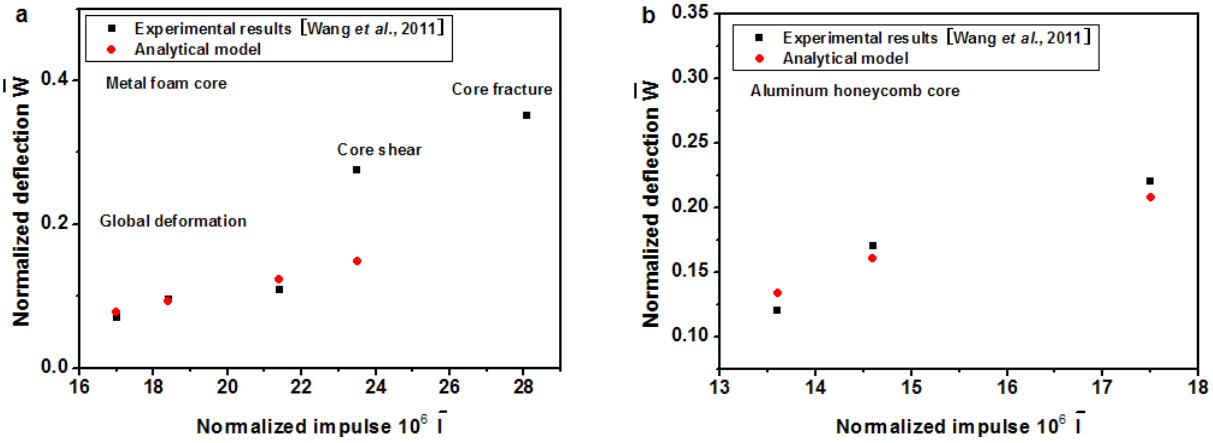

Figure 8 Comparison between the analytical predictions and experimental results by Wang *et al.* [10] for (a) Metal foam core, and (b) aluminum honeycomb core.

Figure 9 shows the contours of plastic strain in the right part of sandwich beam obtained by FE simulation since the deformation is symmetry. Fig. 9a shows the mesh of the model. The impulse $\bar{I} = 4.91\times10^{-6}$. Beam geometrical and material parameters are: h_f=h_b=0.5mm, C=10mm,

σ_p=0.1MPa (γ=2.08), ε_D=0.7, σ_y =75.8MPa. It is seen that during the deformation of the sandwich beam, the foam core is not only compressed, but also bended as the striker velocities decrease to zero, which may be of significant effect on the overall behavior of the sandwich beam. Therefore, the effect of compression and bending of the foam core on global deformation should be considered in the theoretically analysis. In the following discussion, we compare the finite element results with the aforementioned analytical solutions.

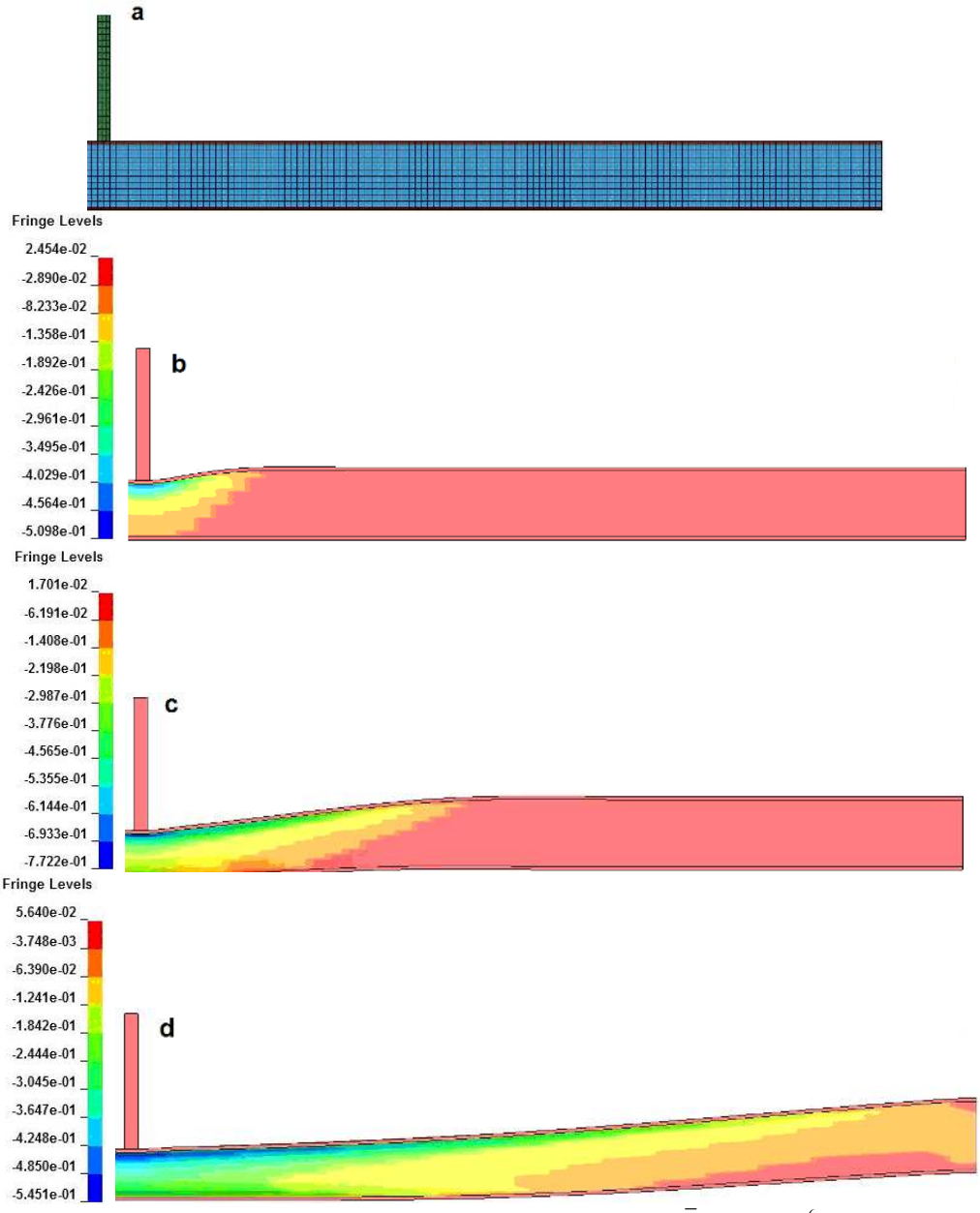

Figure 9 Numerical results for the impact response of the sandwich beam. The impulse $\bar{I} = 4.91\times10^{-6}$, V=20m/s. Beam geometrical and material parameters are: h_f=h_b=0.5mm, C=10mm, σ_p=0.1MPa (γ=2.08), ε_D=0.7, σ_y =75.8MPa. (a) Mesh of the sandwich beam; (b) Distribution of plastic strain when $\bar{t} = 0.15$; (c) Distribution of plastic strain when $\bar{t} = 0.5$; (d) Distribution of plastic strain when $\bar{t} = 1.5$.

Figure 10 shows the comparison of the predicted results from the present model and that of Tilbrook *et al.* (2007), as well as the numerical ones from FE simulation. It is seen that because the shear/bending strength of the core prior to the equalization of the velocities of the front and back faces (that is, in the first and second phases) is ignored, the velocity of the front beam, predicted by Tilbrook *et al.* (red dash-dot lines), is a little slower than the FE results (blue dash lines), whilst the velocity of the back beam is larger than those given by FE simulation. The velocity equivalent reaches in the first phase, and the responses of the sandwich beam goes directly into phase III, which corresponds to Regime A in Fig. 7a. It is seen that the front and back faces reach a higher equal velocity much earlier than the numerical one, which results in the over-estimation of the mid-span deflection of the face-sheets. This great discrepancy further indicates the necessity of considering the shear/bending strength of the core even prior to the equalization of the face velocities.

In our modeling (black solid lines), the velocities of the front and back beams are coincided well with those given by FE simulation. The core densification occurs before the equivalence of beam velocities in the first phase, and the responses of the sandwich beam follow directly into phase III, where the sandwich beam deforms as a single beam, corresponding to Regime B given in Fig. 7b. In phase III, the velocity deviation from FE simulations is due to the assumption made for the core in the analytical modeling, that is, the core is treated rigid after densification. In fact, in FE simulation, at time $t=t_D$, the core densification at the mid-span occurs. However, the other parts of the core have not yet been densified. This is just why no obvious velocity impact discontinuity is observed in the FE results. Comparison between the results given by our model and FE simulation shows that our model can well predict the mid-span deflection of the sandwich beam. It is also noticed that the response of the back beam is postponed in our modeling. This is partly due to the increase of the bending moment of the back beam in our model since the bending strength of the core is considered (Eq. 4). The comparison indicates that our model in treatment of the core deformation is reasonable and could well describe the dynamic responses of sandwich beams under a projectile impact.

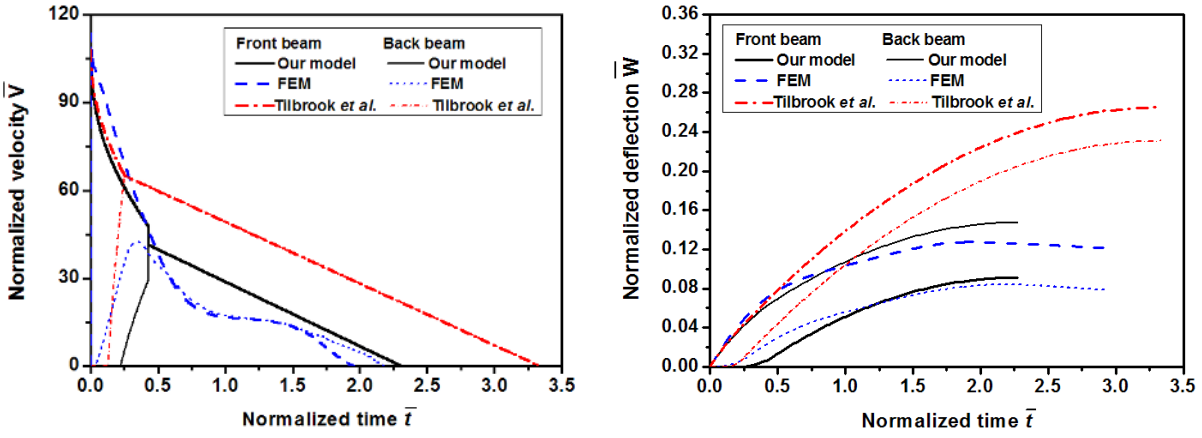

Figure 10 Comparison of analytical predictions of our and Tilbrook models with respect to the data given by FE simulations for normalized mid-span velocity and deflection of front and back face-sheets. The impulse $\bar{I}=9.82\times10^{-6}$, V=40m/s. Beam geometrical and material parameters are: $h_f=h_b$=0.5mm, C=10mm, σ_p=0.1MPa (γ=2.08), ε_D=0.7, σ_y =75.8MPa.

Figs. 11 to 13 give the analytical and FE predictions of the normalized mid-span velocity and deflection of front and back beams under different impulse loadings. The results before the mid-span velocity reaches zero for the first time are given. Seen as Fig. 11, under low impulse loading ($\bar{I}=6.63\times10^{-6}$), the mid-span velocities of the front and back beams reach the equal value in the first phase, and then goes into phase III- system deformation directly, which has the same behavior as that shown in Fig. 7a. The mid-span deflection predicted by our model and FE simulation coincides well with each other. In this situation, the velocity deviation in phase III is due to the theoretical assumption that the beams deform as a system after the velocity equalization. Actually, in the FE simulation, before the velocity equivalence, the front beam makes the decelerated motion, while the back beam accelerated one. At time $t=t_{eq}$, the equalization of the mid-span velocities reaches. Then at the next time, the velocity of the back face will be larger than that of the front face, which results in the traction of the core. At that time, the directions of the pressures act on the face sheets have changed. The back face will make the decelerated motion whilst the front face accelerated one, which results in the equal face velocity a few times later. Then the front and back faces will make the same motion again until all of the kinematic energy is dissipated. This process also indicates that at the first velocity equalization, due to the direction inverse of the face pressures and the large acceleration, the delimitation of the back face with the core maybe happen.

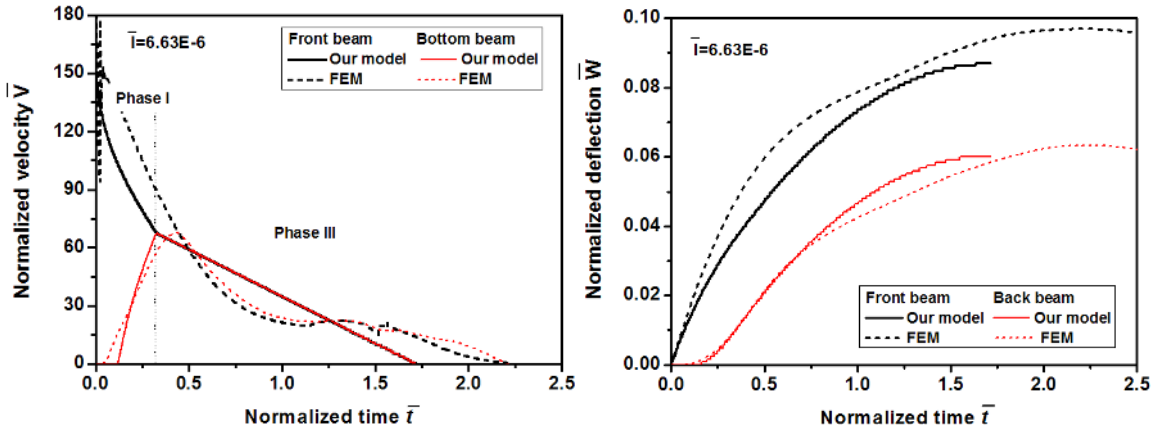

Figure 11 Analytical and FE predictions of normalized mid-span velocity and deflection of front and back face-sheets with V=30m/s. Material and geometrical parameters are: h_f=h_b=0.5mm, C=10mm, σ_p=0.1MPa (γ=2.08), ε_D=0.7, σ_y =75.8MPa.

Along with the increase of the loading impulse ($\bar{I}=9.82\times10^{-6}$, Fig. 12), the densification reaches before the equalization of the beam mid-span velocities, then the responses of the beams follows phase III, as shown in Fig. 7b. It is noticed that the predicted velocity of the back face is the same as that given by FE simulation. But the responses of the front and back beams are not synchronous. The responses of the back beam are postponed. According to Eqs. (26) and (16), the delay time could be determined. However, the mid-span deflection predicted by our model agrees well with those given by FE simulation.

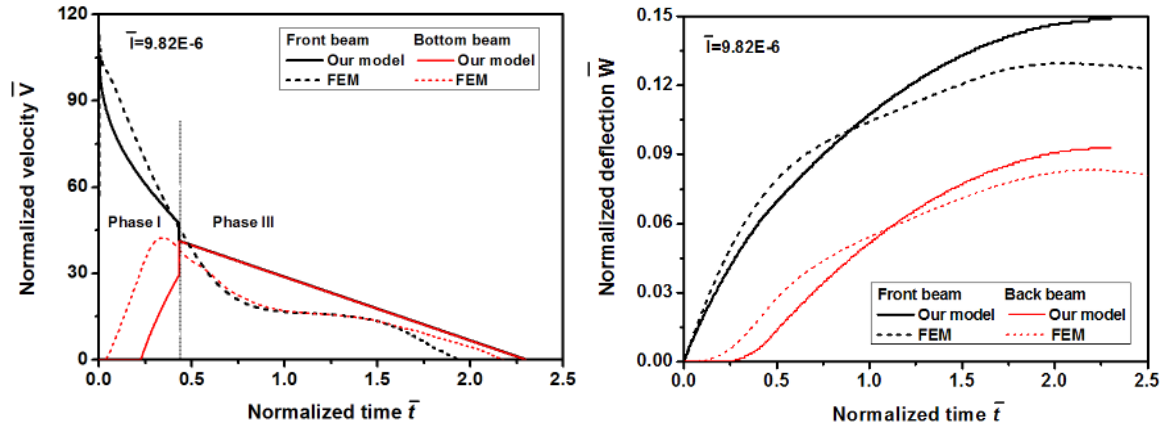

Figure 12 Analytical and FEM predictions of normalized mid-span velocity and deflection of front and back face-sheets with V=40m/s. Material and geometrical parameters are: h_f=h_b=0.5mm, C=10mm, σ_p=0.1MPa (γ=2.08), ε_D=0.7, σ_y =75.8MPa.

Along with the further increase of the loading impulse ($\bar{I}=13.2\times10^{-6}$, Fig. 13), due to the postponed responses of the back beam, the densification occurs before the motion of the back beam, and the responses of the sandwich beam goes directly into phase III. It is seen that the discrepancy between the analytical predictions of mid-span normalized deflection and the numerical ones could be ignored.

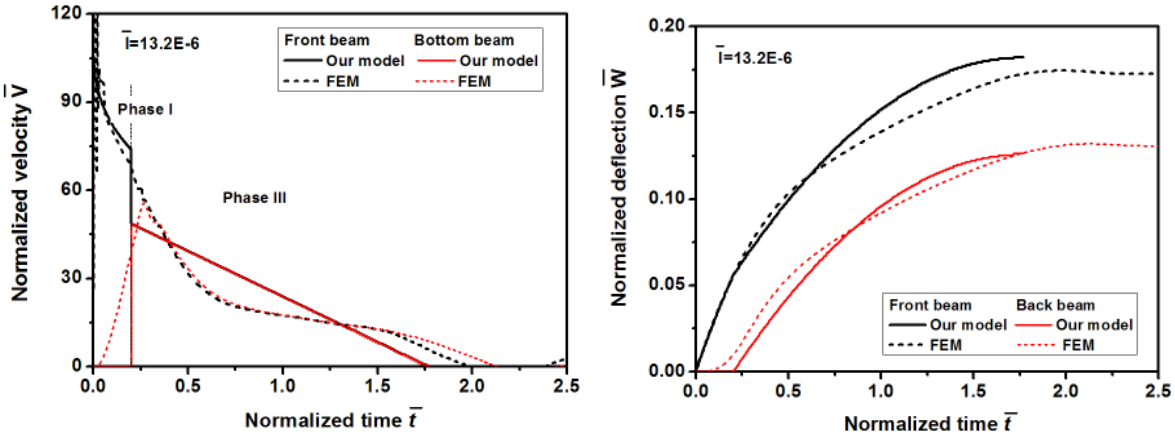

Figure 13 Analytical and FEM predictions of normalized mid-span velocity and deflection of front and back face-sheets with V=60m/s. Material and geometrical parameters are: h_f=h_b=0.5mm, C=10mm, σ_p=0.1MPa (γ=2.08), ε_D=0.7, σ_y =75.8MPa.

Figure 14 shows the comparison between the analytical predictions and numerical simulations for the normalized kinematic energy and plastic energy with respect to the time. The loading impulse $\bar{I}=9.82\times10^{-6}$ (V=40m/s, Fig. 12). It is seen that in phase I, the analytical and numerical ones agree well with each other. In the third phase, the differences are due to the continuously coupling deformation of the face sheets and the core, which is ignored in the analytical modeling. But our model predicts well the final responses of the sandwich beams.

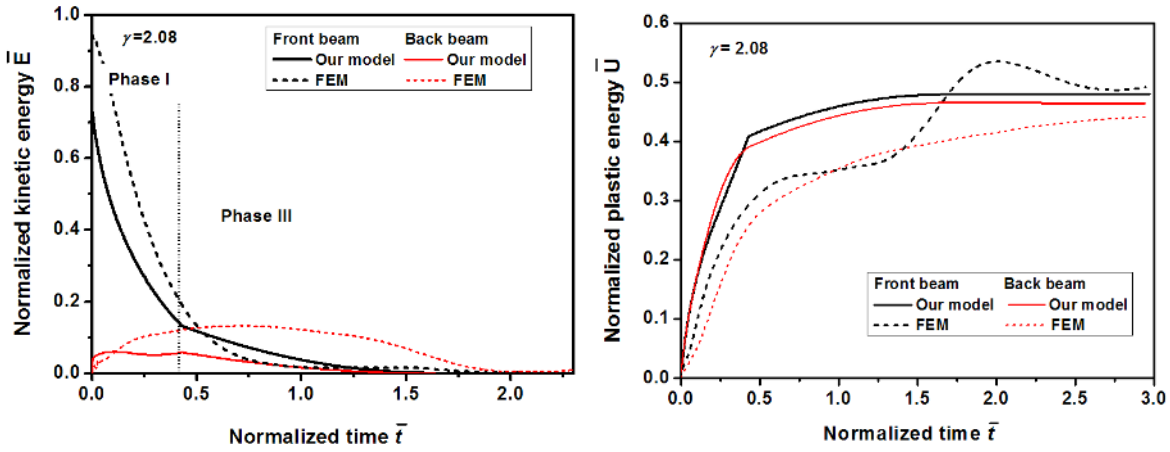

Figure 14 The time histories of normalized kinetic and plastic energies in the face sheets and the foam core of sandwich beams.

Figure 15 gives the normalized mid-span velocity with respect to the time under the same loading impulse but different impacting mass. For light mass impacting, the difference between the initial mid-span velocity of the front beam $\bar{V}_f|_{\bar{t}=0}$ and the equivalent velocity of the face sheets is great, which results in larger mid-span deflection of the front beam. It is seen that under the same impulsive loading, densification at the mid-span of the beam occurs when m_0=0.0125kg (red dash dot lines), which is due to the formation of the concave dent on the front beam in phase I, with the dent width inverse proportion to the impact mass (Eq. 16, mass increasing causing the decreased plastic hinge velocity). So for certain loading impulse, under light mass impacting, the local deformation phenomenon near the impacting zone is predominating. Along with the increase of the impact mass, the value of the equivalent velocity and the time t_{eq} are both decreased. The difference between the initial front beam mid-span velocity $\bar{V}_f|_{\bar{t}=0}$ and the equivalent velocity of the face sheets is decreased, which results in the decreased mid-span deflection of the front beam. That is, along with the increase of impacting mass, the deformation of the sandwich beam is global bending dominated.

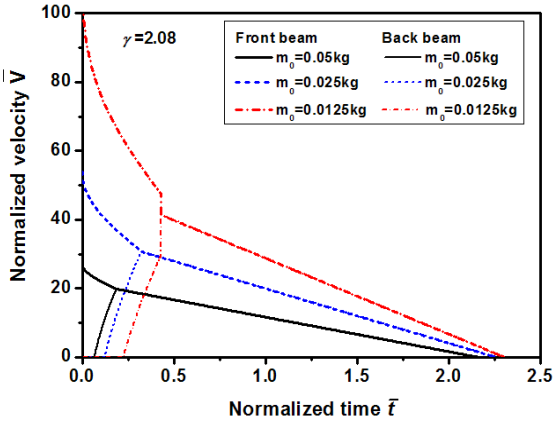

Figure 15 Comparison of normalized front and back face-sheet mid-span velocities versus time under the same impulse loading ($\bar{I}=9.82\times10^{-6}$) but different impact mass.

Figure 16 displays the normalized mid-span velocity and deflection with respect to the time histories for different sandwich beams under the same impulse ($\bar{I}=6.63\times10^{-6}$). For soft core ($\gamma<1$, Fig. 16a), the densification occurs in the phase II and then the front and back beams deform systematically in phase III. During this process, the back beam is assumed un-deformed until densification occurs (our model, solid lines). It is noticed that in the FE simulation, the back face sheet is not stationary although the final deflection of the back beam could be ignored (FE results, dash lines). Along with the increase of the core strength ($\gamma>1$), the equalization of mid-span velocities of beams may happen in the first or second phase, which is then followed by the systematical deformation of the sandwich beam (Figs. 16b and 16c). It is seen that along with the increase of the core strength, the time to the equalization of beam mid-span velocity is decreased, which is due to the accelerated motion of the back beam, but decelerated motion of the front beam. It is seen in all of these situations, our model can well predict the mid-span deflection of the beams.

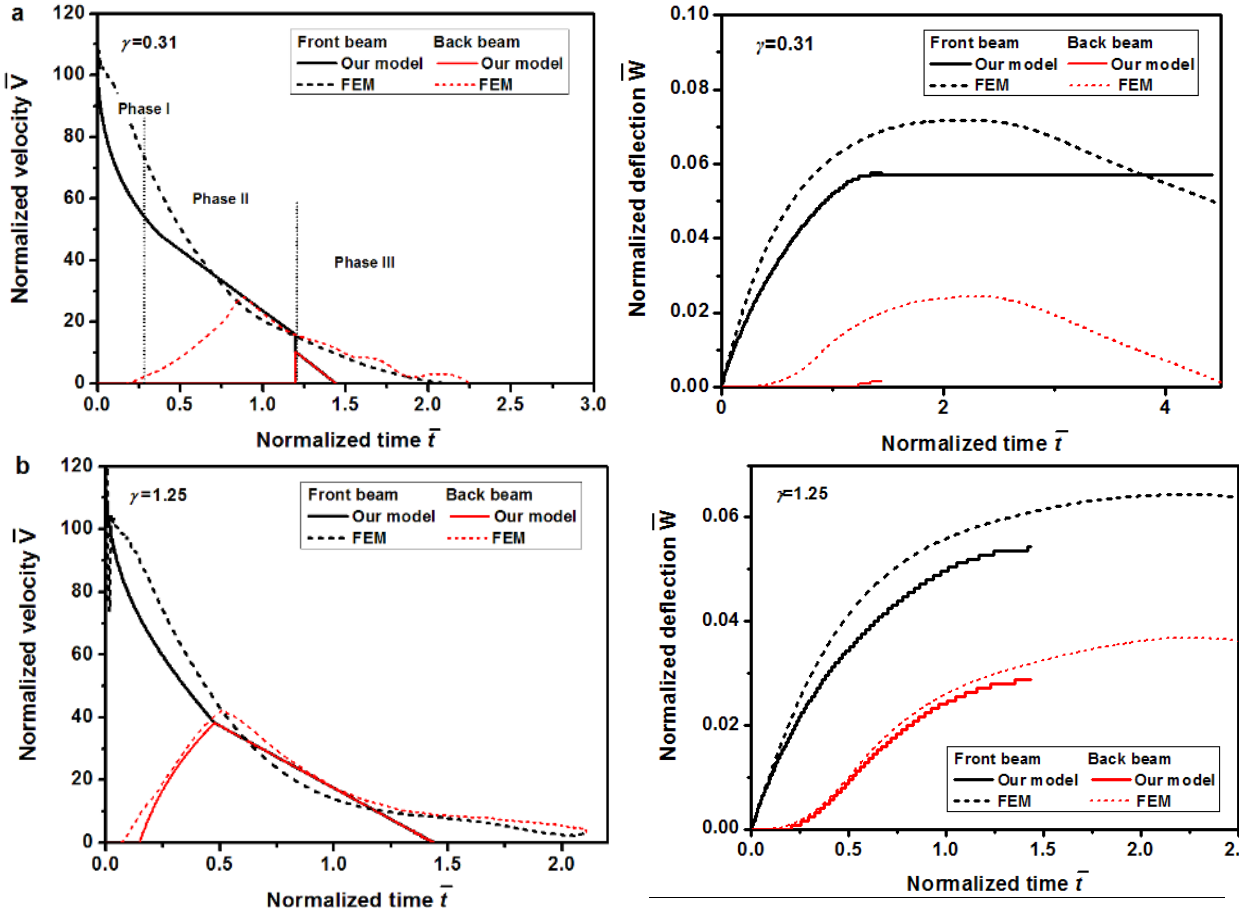

Figure 16 Analytical and FEM predictions of the normalized front and back face-sheet mid-span velocity and deflection versus time for sandwich beams with different strength foam core: (a) s_p =0.01MPa; (b) s_p =0.05MPa; (c) s_p =0.1MPa. Material and geometrical parameters are: h_f=h_b=0.5mm, C=10mm, ε_D=0.7, σ_y =75.8MPa.

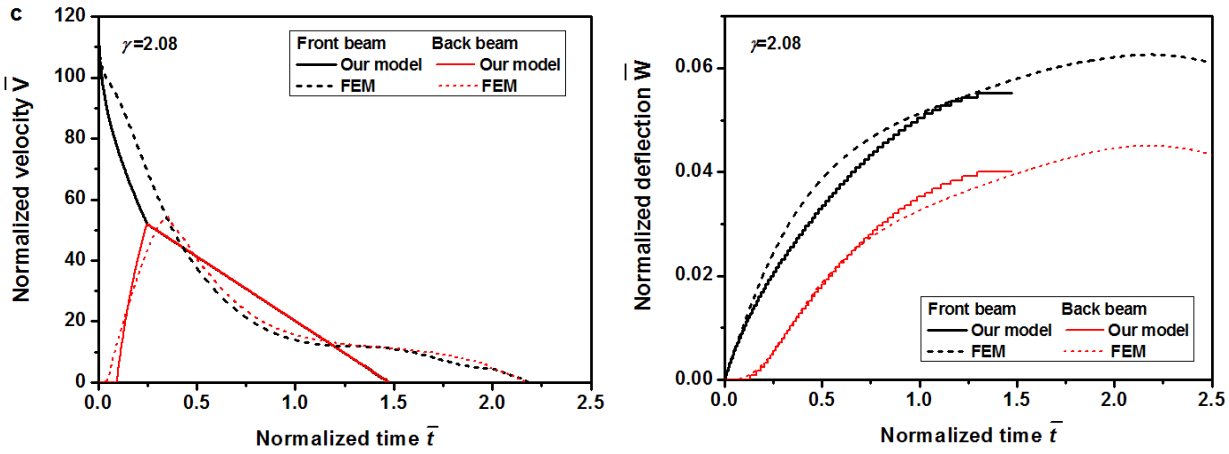

Figure 16 (continued) Analytical and FEM predictions of the normalized front and back face-sheet mid-span velocity and deflection versus time for sandwich beams with different strength foam core: (a) s_p =0.01MPa; (b) s_p =0.05MPa; (c) s_p =0.1MPa. Material and geometrical parameters are: h_f=h_b=0.5mm, C=10mm, ε_D=0.7, σ_y =75.8MPa.

4 CONCLUDING REMARKS

In this paper, a modified beam-spring model is proposed to investigate the dynamic responses of a clamped sandwich beam under impulsive projectile impact. Different from Tilbrook *et al.* (2007), that is, the bending/shear effect of the core is ignored before the velocity equivalence of the face sheets, the bending effects of the core are considered in the whole deformation process of the sandwich beams. Different from beam-spring system on-rigid foundation (Chen and Yu, 2000; Yu *et al.*, 2002), the coupling motion of the front and back beams is considered. The comparison among analytical predictions, experimental data, and numerical simulations shows that our model enables acceptable predictions of the responses of the sandwich beams under mass impact when the foam core makes large global deformation.

It should be pointed out that although the present model is based on small deflection, it has potential to be further developed by incorporating more factors. For instance, large deflections and local deformation characteristic of the foam core are expectable to be incorporated into the model, which will be given in the forthcoming papers.

Acknowledgements The financial supports from the National Science Foundation of China (No. 11272046, 11172033), the National High Technology Research and Development Program of China (863 Program, No. 2013AA030901), the National Basic Research Program of China (973 Program) (2010CB7321004), and 111 project, are acknowledged. The first author also would thanks for the support by a fund from Defense Research and Technology Office, NTU, Singapore, and the Program for New Century Excellent Talents in University (NCET).

References

Fleck, N.A., Deshpande, V.S. (2004). The resistance of clamped sandwich beams to shock loading. ASMA J Appl Mech 71: 386-401.

Xue, Z., Hutchinson, J.W. (2004). A comparative study of blast-resistant metal sandwich plates. Inter J Impact Eng 30: 1283-1305.

Rabczuk, T., Kim, J.Y., Samaniego, E., *et al.* (2004). Homogenization of sandwich structures. Inter J Num Methods Eng 7: 1009-1027.

Liang, Y., Spuskanyuk, A.V., Flores, S.E., *et al.* (2007). The response of metallic sandwich panels of water blast. J Appl Mech 74: 81-99.

Deshpande, V.S., Fleck, N.A. (2005). A one-dimensional response of sandwich plates to underwater shock loading. J Mech Phys Solids 53: 2347-2383.

Taylor, G.I. (1963). The pressure and impulse of submarine explosion waves on plates. The Scientific Papers of G I Taylor, vol. III: Cambridge University Press.

Tilbrook, M., Deshpande, V.S., Fleck, N.A. (2007). The impulsive response of sandwich beams: Analytical and numerical investigation of regimes of behavior. J Mech Phys Solids 54: 2242-2280.

Qin, Q.H., Wang, T.J., Zhao, S.Z. (2009). Large deflections of metallic sandwich and monolithic beams under locally impulsive loading. Inter J Mech Sci 51: 752-773.

Qin, Q.H., Wang, T.J. (2011). Low-velocity heavy-mass impact response of slender metal foam core sandwich beam. Compos Struct 93: 1526-1537.

Wang, Z.H., Lin, J., Ning, J.G., Zhao, L.M. (2011). The structural response of clamped sandwich beams subject to impact loading. Compos Struct 93: 1300-1308.

Liu, Y., Zhang, X.C. (2009). The influence of cell micro-topology on the in-plane dynamic crushing of honeycombs. Int J Impact Eng 36: 98-109.

Liu, Y., Wu, H.X., Wang, B. (2012). Gradient design of metal hollow sphere (MHS) foams with density gradient. Compos part B 43: 1346-1352.

Chen, X.W., Yu, T.X. (2000). Elastic–plastic beam-on-foundation under quasi-static loading. Int J Mech Sci 42: 2261–2281.

Yu, T.X., Chen, X.W., Chen, Y.Z. (2002). Elastic–plastic beam-on-foundation subjected to mass impact or impulsive loading. Comp Struct 80: 1965-1973.

Lopatnikov, S.L., Gama, B.A., Gillespie, Jr J.W. (2007). Modeling the progressive collapse behavior of metal foams. Int J Impact Eng 34: 587-95.

Jones N (1989). Structural Impact. Cambridge: Cambridge University Press9.

LSTC (2007). LS-DYNA keyword user's manual. Livermore Software Technology Corporation.

Appendix A: Clamped monolithic beam under mass impact (Jones, 1989)

In the first phase, considering the symmetric deformation, the right half beam $0 \le x \le L$ is considered. Its transverse velocity is expressed as (Fig. 4a)

$$\dot{w} = \dot{W}(1 - x/\xi) \qquad 0 \le x \le \xi \tag{A1a}$$

$$\dot{w} = 0 \qquad \xi \le x \le L \tag{A1b}$$

where ξ is dependent on the time t and the position x, and the upper dot means the differential with respect to the time t. At the moving plastic hinges ($x=\pm\xi$), the bending moment M_0 is the maximum and the transverse force $Q=0$. The force balance between the two moving plastic hinges along the transverse direction yields

$$m_0\ddot{W} + 2\int_0^{\xi} m_1 \ddot{w} dx = 0 \tag{A2}$$

where m_1 is the mass per length of the beam. Substitution Eq. (A1) into Eq. (A2) leads to

$$m_0\ddot{W} + 2m_1\int_0^{\xi} [\ddot{W}(1 - x/\xi) + \dot{W}x\dot{\xi}/\xi^2] dx = 0 \tag{A3}$$

that is,

$$m_0\ddot{W} + m_1(\ddot{W}\xi + \dot{W}\dot{\xi}) = 0 \tag{A4}$$

Considering $t=0$, $\dot{W} = 0$, and $\xi = 0$, the time integral of Eq. (A4) leads to

$$m_1\dot{W} + m\dot{W}\xi = m_1 V_0 \tag{A5}$$

that is,

$$\dot{W} = V_0/(1 + m_0\xi/m_1) \tag{A6}$$

Considering the moment balance between $x=0$ and $x=\xi$ to the beam midpoint, and the boundary conditions: $M=M_{01}$ at $x=0$; $M= -M_{01}$ and $Q=0$ at $x=\xi$, we have

$$2M_0 - \int_0^{\xi} m_0 \ddot{w} x dx = 0 \tag{A7}$$

Substitution Eq. (A1) into Eq. (A7) yields

$$2M_0 - m\int_0^{\xi}[\ddot{W}(1-x/\xi)+\dot{W}x\dot{\xi}/\xi^2]xdx = 0 \tag{A8}$$

that is,

$$2M_0 - m(\ddot{W}\xi^2/6+\dot{W}\dot{\xi}\xi/3) = 0 \tag{A9}$$

Then Eq. (A9) is rewritten as

$$d(\dot{W}\xi^2)/dt = 12M_0/m \tag{A10}$$

Integrating Eq. (A10) and considering when t=0, ξ=0, we have

$$t = m\dot{W}\xi^2/12M_0 \tag{A11}$$

Combining with Eq. (A6), we have

$$t = mm_1V_0\xi^2/[12M_0(m_1+m\xi)] \tag{A12}$$

Differentiating Eq. (A12) with respect to the time t, we obtain the traveling velocity of the plastic hinges, that is

$$\dot{\xi} = 12M_0(m_1+m\xi)^2/[mm_1V_0\xi(2m_1+m\xi)] \tag{A13}$$

Since no transverse displacement occurs before the moving plastic hinge arrives at $t(x)$, when $t \geq t(x)$, the transverse displacement is determined by

$$w = \int_{t(x)}^{t}\dot{w}dt \tag{A14}$$

where $t(x)$ is obtained according to Eq. (A12) by letting ξ=x.

Let $\dot{\xi} = d\xi/dt$, combining with Eq. (A1), Eq. (A14) is rewritten as

$$w = \int_x^{\xi}\dot{w}d\xi/\dot{\xi} \tag{A15}$$

Substitution of Eqs. (A1), (A6), (A13) into (A15) yields

$$w = \int_x^{\xi}\frac{V_0(1-x/\xi)mm_1V_0\xi(2m_1+m\xi)d\xi}{(1+m\xi/m_1)12M_0(m_1+m\xi)^2} \tag{A16}$$

Integration the above equation, we have

$$w = \frac{m_1^2 V_0^2}{24 m M_0}\left[\frac{1+\beta}{(1+\alpha)^2} - \frac{1+2\beta}{1+\beta} + \frac{2\beta}{1+\alpha} + 2\ln\frac{1+\alpha}{1+\beta}\right] \tag{A17}$$

where $\alpha = m\xi / m_1$, $\beta = mx / m_1$.

In the second phase (Fig. 4c), it assumes that the corresponding transverse displacement field obeys

$$w_2 = \left(L - x\right)\theta \tag{A18}$$

The energy conversation leads to

$$4M_0\theta = m_0 V_0^2\left(1 + 2m_f L / 3m_0 - x\right) / \left[2\left(1 + m_f L / m_0\right)^2\right] \tag{A19}$$

According to Eqs. (A18) and (A19), we have

$$w_2 = m_0 V_0^2 L\left(1 + 2m_f L / 3m_0\right)\left(1 - x / L\right) / \left[8M_0\left(1 + m_f L / m_0\right)^2\right] \tag{A20}$$